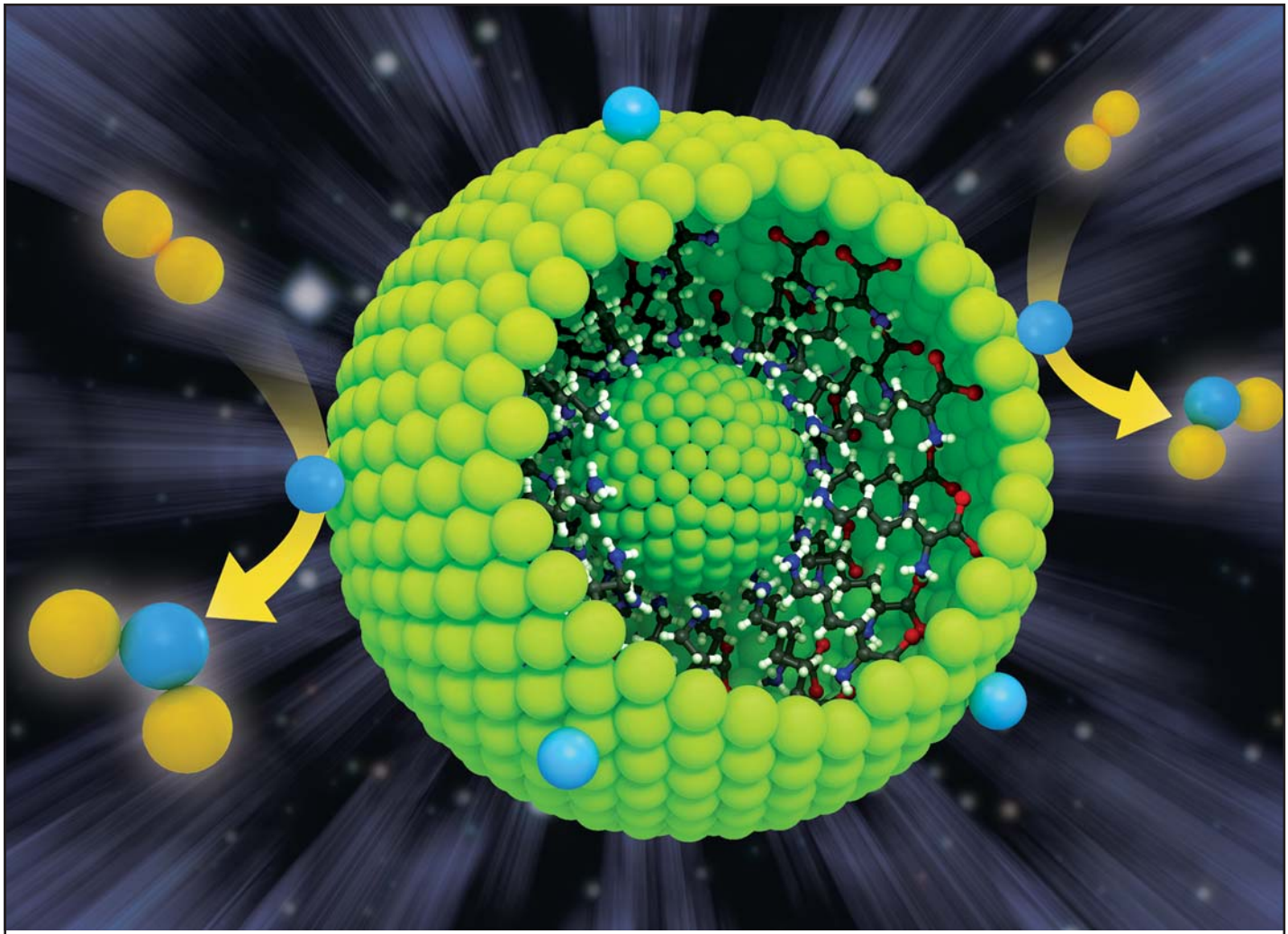

Research highlight from Jong-Heun Lee's group at Korea University in Korea and Guozhong Cao's group at University of Washington in USA.

Title: Template-free solvothermal synthesis of hollow hematite spheres and their applications in gas sensors and Li-ion batteries

Fe_3O_4 hollow spheres were prepared by amino-acid-mediated solvothermal reaction, which were converted into nearly monodisperse Fe_2O_3 hollow spheres with nano-scale thinness by heat treatment. The well-defined hollow Fe_2O_3 spheres showed significantly enhanced C_2H_5OH sensing characteristics and promising Li-ion intercalation behavior.

As featured in:

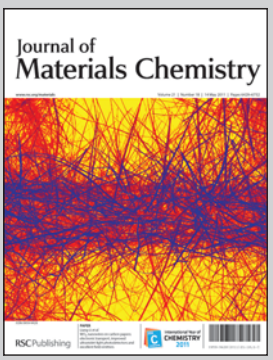

See H.-J. Kim *et al.*,
J. Mater. Chem., 2011, **21**, 6549.

RSC Publishing

www.rsc.org/materials

Registered Charity Number 207890

Journal of Materials Chemistry

Dynamic Article Links

Cite this: J. Mater. Chem., 2011, 21, 6549

www.rsc.org/materials

PAPER

Template-free solvothermal synthesis of hollow hematite spheres and their applications in gas sensors and Li-ion batteries†

Hyo-Joong Kim,[a] Kwon-Il Choi,[a] Anqiang Pan,[bc] Il-Doo Kim,[d] Hae-Ryong Kim,[a] Kang-Min Kim,[a] Chan Woong Na,[a] Guozhong Cao*[b] and Jong-Heun Lee*[a]

Received 18th October 2010, Accepted 12th January 2011
DOI: 10.1039/c0jm03516e

Magnetite (Fe_3O_4) hollow spheres were prepared by solvothermal reaction of ethanol solution containing Fe-acetate and L-lysine, and were subsequently transformed into hematite (Fe_2O_3) hollow spheres with nanoscale (20–30 nm) thin shells by heat treatment at 500 °C for 2 h. Both the as-prepared and heat-treated hollow spheres contained another small sphere within each shell, which was attributed to the following solvothermal self-assembly reactions: (1) the nucleation of Fe_3O_4 spheres, (2) lysine capping on the nuclei, (3) the growth of lysine-capped particles by cross-linking between lysine molecules, and (4) the formation of Fe shell layers by the interaction between Fe ions and outer lysine molecules. In the assembly reaction, L-lysine with amino and carboxyl radicals played the key role. The heat-treated Fe_2O_3 hollow spheres showed significantly enhanced C_2H_5OH sensing characteristics and promising Li-ion intercalation behaviors.

Introduction

Hematite (Fe_2O_3) hollow spheres have been an attractive material platform with potential applications in the fields of drug delivery, energy storage, catalyst, magnetic storage media and gas sensors.[1–6] In the latter application, the rapid and effective diffusion of analyte gas to the entire sensing surface through thin and semi-permeable shells is known to greatly enhance both gas sensitivity and response speed simultaneously.[7,8] Moreover, hollow spheres with high surface area and nano-porous shells are also advantageous for achieving high discharge capacity and coulombic efficiency due to the short diffusion length of Li^+.[2,9] The preparation of well-defined Fe_2O_3 hollow spheres is also essential to enhance the performance of other applications.

The chemical routes to prepare Fe_2O_3 hollow spheres are divided into two categories according to the use of templates. The use of spherical templates is a facile approach to attain hollow morphology. For example, after coating of the Fe-precursors on polystyrene spheres and subsequent conversion of the precursor layer into metal oxide,[10–13] the core templates are removed by thermal decomposition. The chemical steps of template-based approaches can be simplified by employing the one-pot reaction including both the formation of templates and precursor coating. The representative templates formed during one-pot reaction are the glucose-condensed hydrocarbon spheres[14] and microbubbles.[2,15] The representative template-free approaches are polyoxometalate-assisted, forced hydrolysis,[16] microwave hydrothermal reaction,[17] sonochemical reaction,[18] ligand-assisted hydrothermal reaction[19] and Ostwald ripening.[20]

In this contribution, nearly monodisperse Fe_3O_4–hydrocarbon composite spheres were prepared by amino acid (L-lysine)-assisted solvothermal self-assembly reaction. These spheres were converted into Fe_2O_3 hollow spheres with ~30 nm thick shells by heat treatment. To the best of the authors' knowledge, the amino acid-mediated solvothermal preparation of Fe_2O_3 hollow spheres without templates has never been reported. The formation mechanism of Fe_3O_4 hollow spheres was investigated in relation to the self-assembly reaction and the gas sensing and Li-ion battery characteristics of Fe_2O_3 hollow spheres were investigated for their potential applications.

Experimental

Preparation

The Fe_3O_4 hollow spheres were prepared by solvothermal self-assembly reaction. In 50 ml of anhydrous ethanol was dissolved 0.0870 g of iron(II) acetate ($Fe(CH_3CHOO)_2$, 99.995%, Sigma-Aldrich Co.). After adding 0.0146 g of L(+)-lysine ($C_6H_{14}N_2O_2$,

[a]Department of Materials Science and Engineering, Korea University, Seoul, 136-713, Republic of Korea. E-mail: jongheun@korea.ac.kr
[b]Department of Materials Science and Engineering, University of Washington, Seattle, Washington, 98195, USA. E-mail: gzcao@u.washington.edu
[c]Department of Materials Science and Engineering, Central South University, Hunan, 410083, China
[d]Optoelectronic Materials Center, Korea Institute of Science and Technology, Seoul, 130-650, Republic of Korea

† Electronic supplementary information (ESI) available: XPS spectra, EDS results, and particle size distribution of hollow spheres, SEM and TEM images of materials and sensor surface, DTA/TG results, X-ray diffraction patterns, and gas sensing transients. See DOI: 10.1039/c0jm03516e

≥98%, Sigma-Aldrich Co.), the solution was homogenized by ultrasonic transduction and vigorous stirring. Subsequently, the stock solution was transferred to a Teflon-lined stainless steel autoclave (volume: 100 cm^3), which was then sealed and heated at 200 °C for 4 h. After cooling, the resulting product was washed five times with ethanol using a centrifuge and then dried at 70 °C for 1 day. The as-prepared powders were Fe_3O_4 hollow spheres, which were oxidized into Fe_2O_3 by heat treatment at 450–600 °C for 2 h. In order to investigate the effect of Pt loading on the gas sensing characteristics, the Pt-doped hollow Fe_2O_3 spheres (Pt/Fe_2O_3 = 0.70 wt%) were prepared by the solvothermal reaction of stock solution containing $PtCl_4$ (98%, Sigma-Aldrich Co.), $Fe(CH_3CHOO)_2$, and L(+)-lysine and subsequent heat treatment. For comparison, Fe_2O_3 solid spheres were also synthesized by solvothermal reaction of C_2H_5OH solution containing only $Fe(CH_3CHOO)_2$, followed by heat treatment at 500 °C for 2 h. For further comparison, Fe_2O_3-agglomerated nanoparticles were prepared by the heat treatment of carbonate precipitates at 500 °C for 2 h. 4.80 g of $(NH_4)_2CO_3$ was dissolved in 100 ml of distilled water heated at 60 °C. 4.04 g of $Fe(NO_3)_3$ (>98%, Sigma-Aldrich Co.) was dissolved in 100 ml of distilled water at 40 °C and the solution was gradually dripped into the aforementioned $(NH_4)_2CO_3$ (Sigma-Aldrich Co.) aqueous solution for precipitation. After precipitation, the solution was stirred for 2 h at 60 °C. The precipitates were washed with distilled water and then ethanol. After drying at room temperature for 24 h, the precursors were converted into Fe_2O_3-agglomerated nanoparticles by heat treatment 500 °C for 2 h.

Characterization

The phase and crystallinity of the powders were analyzed by X-ray diffraction (XRD, Rigaku D/MAX-2500V/PC), the morphologies of the precursors and hollow powders by field-emission scanning electron microscopy (FE-SEM, S-4800, Hitachi Co. Ltd., Japan) and transmission electron microscopy (TEM, FEI Tecnai 20), and the surface areas of the powders by using the Brunauer–Emmett–Teller (BET) method (Tristar 3000, Micromeritics Co. Ltd.).

Gas sensing characteristics

The as-prepared precursors were prepared in a paste form and applied to an alumina substrate having two Au electrodes. The sensor element was heat treated at 500 °C for 2 h to decompose the organic content of the paste. The sensor was placed in a quartz tube and the temperature of the furnace was stabilized at 400 °C. A flow-through technique with a constant flow rate of 500 cm^3 min^{-1} was used. The gas response ($S = R_a/R_g$, R_a: resistance in air, R_g: resistance in gas) was measured at 400 °C. The dc 2-probe resistance of the sensor was measured using an electrometer interfaced with a computer.

Li-ion battery characteristics

The Fe_2O_3 hollow powders heat-treated at 450 °C were ground with conductive carbon black (super P, TIMCAL) in mortar and polyvinylidene fluoride (PVDF, ARKEMA) dissolved in *N*-methyl-2-pyrrolidone (NMP, Sigma) was added to the mixture of active materials and super P. The weight ratio of active materials, super P and PVDF in NMP solvent, was 8 : 1 : 1. The mixture was stirred for 24 hours and the resulting slurry was coated on copper foil. The electrode was punched from the aluminium foil into circles of 13 mm diameter. The electrodes were dried under vacuum at 80 °C overnight. For assembling the button cells, the metal Li was used as the counter electrode and 1 M $LiPF_6$ (Battery grade, Novolyte Technologies Inc.) dissolved in a 1 : 1 (volume ratio) mixture of ethylene carbonate/dimethyl carbonate was employed as electrolyte. All the assembling processes were carried out in an Ar-filled glove box. The cell test was carried out at a current density of 100 mA g^{-1} using an Arbin battery testing system (BT-2000, Arbin Instruments, USA).

Results and discussion

X-Ray diffraction (XRD)

The as-prepared powders after solvothermal reaction at 200 °C were identified as crystalline Fe_3O_4 phase (JCPDS # 19-0629) (Fig. 1a). After heat treatment at 450 °C for 2 h, the powders were transformed into Fe_2O_3 with minor Fe_3O_4 (Fig. 1b). Pure Fe_2O_3 phase (JCPDS 33-0664) was attained by further increasing the heat-treatment temperature to 500 and 600 °C (Fig. 1c and d). The XRD pattern of γ-Fe_2O_3 (JCPDS 39-1346) is also similar to that of Fe_3O_4. In X-ray photoelectron spectroscopy (XPS) analysis, the binding energies for the Fe $2p_{1/2}$ and Fe $2p_{3/2}$ peaks of as-prepared hollow spheres were ~0.3 eV lower than those of Fe_2O_3 hollow spheres heat-treated at 500 °C for 2 h, respectively (see ESI, Fig. S1†). This indicates that the as-prepared specimen in Fig.1a can be identified as Fe_3O_4 rather than γ-Fe_2O_3.[21] The primary particle sizes of the as-prepared Fe_3O_4 hollow spheres and 500 °C heat-treated Fe_2O_3 hollow spheres calculated by Scherrer's equation were 10.7 ± 0.9 and 32.8 ± 4.2 nm, respectively.

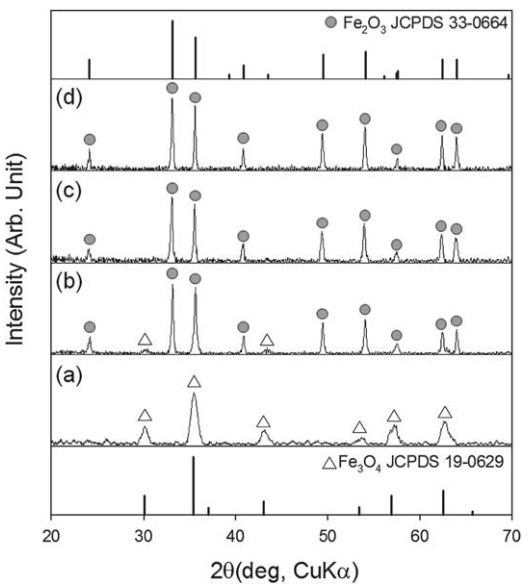

Fig. 1 X-Ray diffraction (XRD) patterns of (a) the as-prepared powders after solvothermal reaction at 200 °C, and of those heat-treated for 2 h at (b) 450 °C, (c) 500 °C, and (d) 600 °C.

SEM and TEM analysis

Uniform and nearly mono-disperse Fe_3O_4 spheres were obtained by the solvothermal reaction (Fig. 2a and b). Smaller particles (size: ~300 nm) were also observed, which lead to the bimodal particle size distributions (Fig. S2†). The size of the spheres ranged from 600 to 1200 nm. A few broken spheres showed a shell morphology (arrows in Fig. 2a and b), which indicated the formation of hollow spheres. Closer TEM observation confirmed that the as-prepared Fe_3O_4 spheres were hollow (Fig. 2c) and contained another small sphere within each hollow sphere, as shown in the arrowed regions in Fig. 2c and d. The ring diffraction pattern suggests that the hollow spheres were poly-crystalline Fe_3O_4 (inset in Fig. 2c). The outer shells of the hollow spheres were 40–70 nm thick (see for example, Fig. 2e) and the primary particles were ~10 nm in diameter (Fig. 2f).

The spherical morphology (Fig. 3a) and the coexistence of smaller particles (Fig. 3b and S2b†) remained similar after heat treatment at 500 °C for 2 h and the sizes of the Fe_2O_3 spheres decreased slightly (500–1000 nm). The shells of the heat-treated Fe_2O_3 hollow spheres became more distinct (Fig. 3c) and their thickness was decreased to 24–33 nm (Fig. 3d). The small spheres within the hollow shells became significantly smaller upon heat treatment (Fig. 2c and 3c). Well-developed crystalline structures were found in the local area (Fig. 3e). Two lattice planes with interplanar distances of 2.71 and 3.74 Å and an angle of 46.4° were observed in the lattice fringe (Fig. 3f), which corresponded to the (012) and (104) planes of the SnO_2 cassiterite (rutile) crystal structures, respectively.

The solvothermal reaction of the ethanol solution containing $Fe(CH_3CHOO)_2$ in the absence of L(+)-lysine produced spheres with solid inner structures (Fig. S3a and b†). This solid morphology remained after heat treatment at 500 °C for 2 h (Fig. S3c and d†), which indicated that L(+)-lysine plays a key role in the formation of hollow structures. Abundant carbon and nitrogen components were found in the energy-dispersive X-ray spectroscopy (EDS) analyses over the entire region of the as-prepared spheres (Fig. S4†). Some of the carbon content could be attributed to the residual solvent or the specimen grid for TEM observation. However, the substantial nitrogen concentration

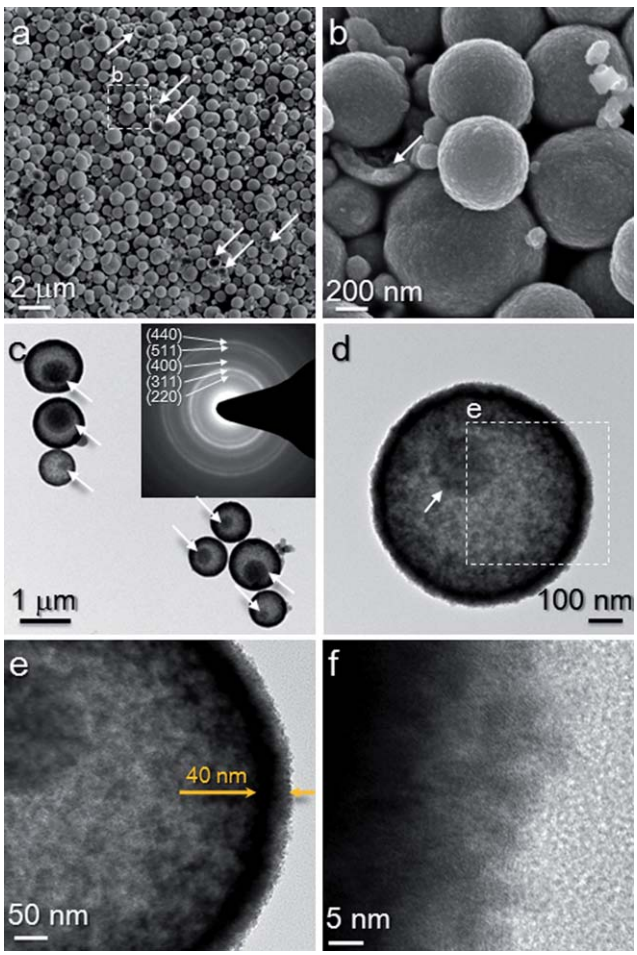

Fig. 2 Morphologies of the as-prepared Fe_3O_4 hollow spheres after solvothermal reaction at 200 °C: (a) low magnification SEM image; (b) high magnification SEM image of the rectangular area in (a), (c) TEM image and ring diffraction pattern, (d) TEM images of a single hollow sphere, (e) high magnification TEM image of the rectangular area in (d), and (f) high magnification image near the surface of the hollow sphere.

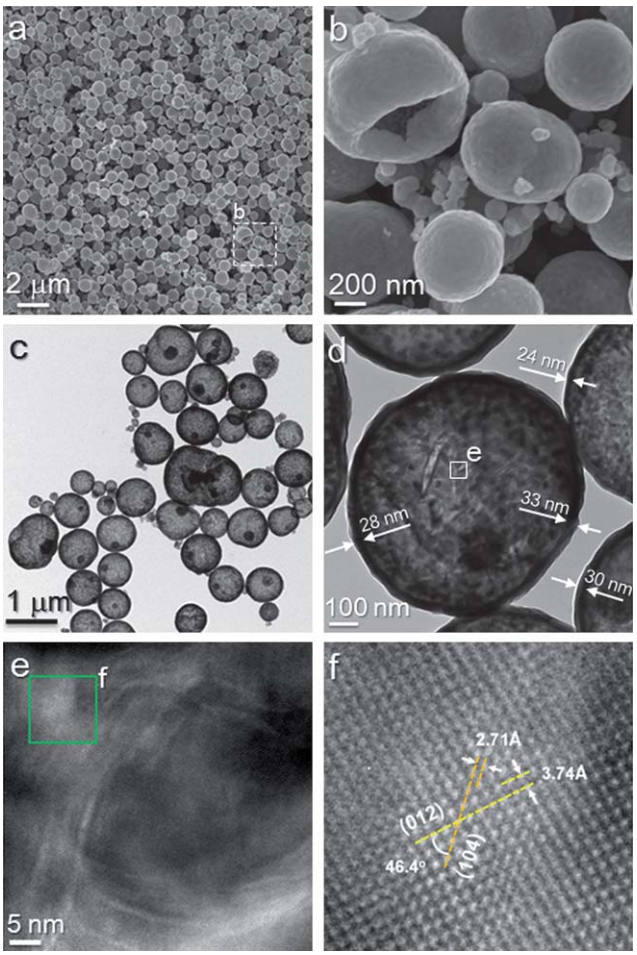

Fig. 3 Morphologies of the Fe_2O_3 hollow spheres after heat treatment at 500 °C for 2 h: (a) low magnification SEM image, (b) high magnification SEM image of the rectangular area in (a), (c) TEM image of the hollow spheres, (d) TEM image of a hollow sphere, (e) high magnification TEM image of the rectangular in (d), and (f) lattice fringes from (012) and (104) planes (rectangular region in (e)).

emanated from L(+)-lysine or its modified components within a Fe_3O_4 sphere. In particular, the nitrogen concentration was higher in the area of the small sphere within a large hollow sphere (Fig. S4†), which demonstrated that L(+)-lysine plays a role in the formation of small spheres or cross-links between the outer shell and the inner sphere. After heat treatment at 500 °C for 2 h, the nitrogen concentration within the Fe_2O_3 spheres was reduced to a negligible level by the decomposition of amino acid-related components (Fig. S5†), which was confirmed by DTA/TG analysis (Fig. S6†).

The formation of hollow spheres during the solvothermal reaction was further investigated from the Fe_3O_4 and Fe_2O_3 hollow spheres prepared by focused ion beam (FIB) treatment (Fig. 4). As found in the TEM observations, the size of the small sphere within a large hollow shell was decreased by heat treatment at 500 °C for 2 h, suggesting that this small sphere (Fig. 4a and b) may have consisted of some organic contents such as L(+)-lysine, as well as Fe-precursor, although further study is necessary to confirm this.

The small inner sphere was connected with the outer Fe_3O_4 shell (arrows in Fig. 4a), for reasons which have not yet been fully elucidated. However, one possible explanation is that the inner sphere and outer shell were connected with each other by the mediation of L(+)-lysine. The L(+)-lysine structure comprises one amine and two carboxyl groups, which provide both positive ($–NH_2^+$) and negative ($–COO^-$) ending groups. This amphiphilic nature may enable the electrostatic connection between lysine molecules. The peptide bond between NH_2 and COOH groups can be also considered as the reason for the interaction between lysine molecules.[22,23] Moreover, both amino and carboxyl groups are capable of coordinating with transition metal ions in oxides.[24–26] These reports indicate the versatile roles of lysine: (1) the capping of Fe_3O_4 core spheres, (2) the elongation of lysine chains by electrostatic cross-linking, and (3) the interaction with Fe ions. Indeed, in the as-prepared Fe_3O_4 spheres, a substantial amount of nitrogen was observed not only near the inner spheres but also in the regions between the outer shell and the inner sphere. This strongly supports the formation of a lysine-mediated network between the core spheres and the outer shells. In both the Fe_3O_4 and Fe_2O_3 spheres, the outer surfaces of the outer shells were very smooth and clean, while the inner surfaces of the outer shells showed very rough structures with a number of small protrusions (Fig. 4), which may have resulted from the connection between the inner sphere and the outer shell.

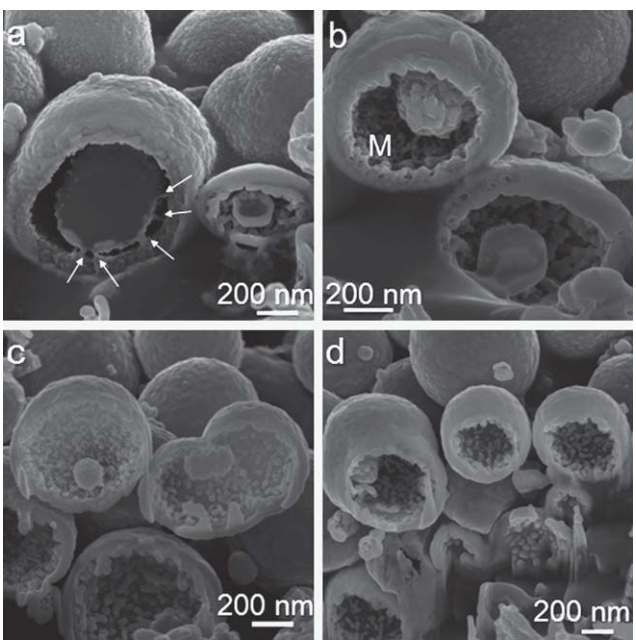

Fig. 4 Inner morphologies of (a), (b) the as-prepared Fe_3O_4 spheres and (c), (d) the Fe_2O_3 spheres after heat treatment at 500 °C for 2 h. The specimens were prepared by focused ion beam (FIB) treatment.

To study the intermediate stages of reaction, the morphologies of products prepared from the same precursor solution for shorter solvothermal-reaction time (0.5, 1, and 2 h) were observed (Fig. S7†). The particles after reaction for 0.5–1 h (Fig. S7a and b†) were not spherical and smaller than those prepared for 4 h (Fig. 2). These particles were changed into larger spherical ones after reaction for 2 h (Fig. S7c†). Taking into account the presence of nitrogen between the core spheres and the outer shells and the evolution of particle size and morphology at the beginning and intermediate stages of reaction, the formation mechanism of the Fe_3O_4 hollow spheres can be given as shown in Fig. 5. Spherical Fe_3O_4 nuclei were formed at the initial reaction stage (Fig. 5a). This is reasonable considering that the Fe_3O_4 spheres with solid inner structures had been prepared by solvothermal reaction in the absence of L-lysine. The spherical nuclei were then capped by the interaction of the amino or carboxyl radical with L(+)-lysine (Fig. 5b). In this stage, Fe ions still existed in the solution and the spherical nuclei could be coarsened. However, the growth reaction was limited because the nuclei were capped with L-lysine.[27] The capped lysine layer could grow either by the electrostatic cross-linking between lysine molecules or by a peptide bond between NH_2 and COOH groups[22,23] (Fig. 5c), in a step which determined the apparent size of the hollow spheres. Due to the amphiphilic nature of lysine, the Fe ions in the solution could also adhere to the end of the outer lysine molecule, which led to the coating of Fe ions with the shell configuration (Fig. 5d). In this stage, the concentration of Fe ions was smaller than that at the initial stage of reaction because a substantial amount of the Fe source had already been consumed in the nucleation. This facilitated the gradual coating of a very thin Fe precursor layer in a well-defined manner. Accordingly, the well-defined Fe_3O_4 hollow spheres with ultrathin (40–70 nm) shell was attributed to the two-stage reaction of the Fe sources under the mediation of L-lysine. The Fe_2O_3 hollow spheres were formed by the decomposition of L(+)-lysine and its related components (Fig. 5e).

Gas sensing characteristics

In order to investigate the effect of hollow morphology and catalyst loading on the gas sensing behaviors, four different

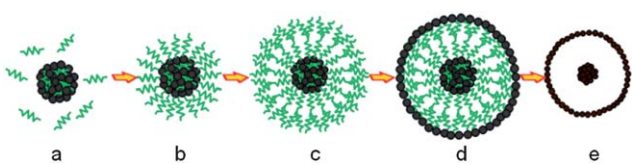

Fig. 5 Formation mechanism of the Fe_3O_4 and Fe_2O_3 spheres.

sensors were fabricated using undoped Fe_2O_3 hollow structures, Pt-doped Fe_2O_3 hollow structures, Fe_2O_3 spheres with solid inner structures, and Fe_2O_3-agglomerated nanoparticles. The Pt-doped Fe_2O_3 hollow spheres were slightly smaller than undoped Fe_2O_3 hollow spheres (Fig. S8†). From EDS analyses, the Pt components were found throughout the whole Fe_2O_3 hollow structures (Fig. S9†). The size of the primary particle size within the Fe_2O_3-agglomerated nanoparticles ranged from 30 to 40 nm (Fig. S10†). The precursors prepared by solvothermal reactions (hollow and solid spheres) were identified as crystalline Fe_3O_4, while the precursor prepared by carbonate precipitation could not be identified (Fig. S11†). All the precursors were converted into phase-pure Fe_2O_3 by heat treatment at 500 °C for 2 h (Fig. S12†).

The undoped and Pt-doped Fe_2O_3 hollow spheres showed selective detection to C_2H_5OH. For example, the response (R_a/R_g) of undoped Fe_2O_3 hollow spheres to 100 ppm C_2H_5OH was 2.55 at 400 °C, which was significantly higher than those to 100 ppm H_2 and 100 ppm CO (1.51 and 1.10). The Fe_2O_3 spheres with solid inner structures and agglomerated nanoparticles showed negligible responses to H_2 and CO. Thus, the C_2H_5OH sensing characteristics of the four different sensors were compared. The sensor resistances were decreased upon exposure to 5–100 ppm C_2H_5OH and were recovered to original resistance upon exposure to air (Fig. S13†).

At the sensing temperature of 300 °C, the gas responses of the undoped and Pt-doped Fe_2O_3 hollow spheres to 5–100 ppm C_2H_5OH ranged from 1.2 to 2.0 (Fig. 6b), while those of the Fe_2O_3 solid spheres and agglomerated nanoparticles were negligible (data not shown). As the sensor temperature was increased to 400 °C, the sensor responses of the undoped and Pt-doped Fe_2O_3 hollow spheres increased and the gas sensing behaviors of the four different sensors began to diverge significantly (Fig. 6a). The increase of gas response by increasing the sensor temperature was attributed to the enhanced oxidative interaction of ethanol with negatively charged surface oxygen (O^-). Upon exposure to 5–100 ppm C_2H_5OH, the gas responses of the agglomerated nanoparticles and of the solid spheres ranged from 1.10 to 1.32 and from 1.19 to 1.67, respectively. In contrast to these two counter parts, the gas responses of the undoped hollow spheres are significantly higher (1.41–2.55). The gas response was enhanced further to 1.77–3.72 by doping with Pt catalyst.

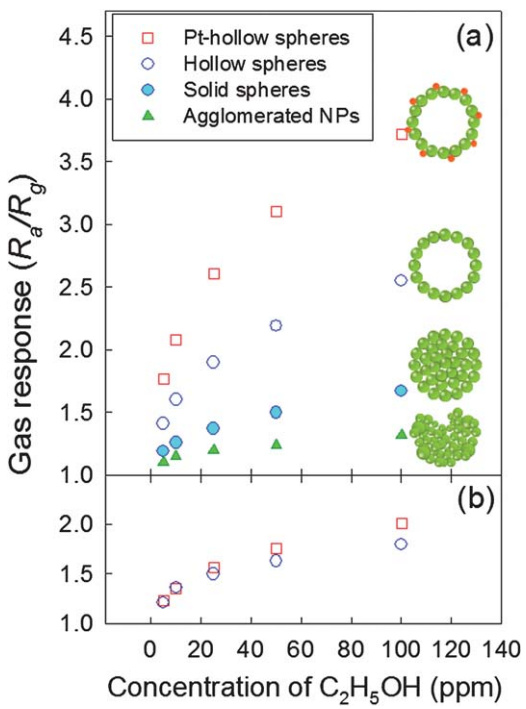

Fig. 6 C_2H_5OH sensing characteristics of the Pt-doped Fe_2O_3 hollow spheres, Fe_2O_3 hollow spheres, Fe_2O_3 solid spheres, and Fe_2O_3-agglomerated nanoparticles at the sensing temperatures of (a) 400 °C and (b) 300 °C.

When the agglomerates of the primary particles were large and dense, the pores between the primary particles become small, which may have hampered the diffusion of analyte gases onto the entire sensor surface.[28,29] Moreover, the tortuous configuration of the pore channels may have hindered the gas diffusion. Therefore, only the primary particles located in the outer region of the secondary agglomerates or the spheres contributed to the gas sensing reaction, while the primary particles located in the inner part became inactive, which reduced the gas response.[30] Indeed, it has been reported that the gas response of an agglomerated configuration of primary particles is significantly smaller than that of a well-dispersed configuration of nanostructures.[31–33] In this framework, the high gas response of the Fe_2O_3 hollow spheres in the present study was attributed to the effective diffusion of analyte gas to the entire sensing surface *via* thin shells. This mechanism is supported by the literature reports of an enhanced gas response by employing hollow structures.[7,28,33–36]

The loading of Pt catalyst is also known to enhance the gas response of semiconductor-type gas sensors by activating a surface reaction between negatively charged surface oxygen and a reducing gas.[37] The BET surface areas of the undoped and Pt-doped Fe_2O_3 hollow spheres after heat treatment at 500 °C for 2 h were 21.5 and 22.4 $m^2\ g^{-1}$, respectively. These similar values support the catalytic activation by Pt as the driver for the enhanced gas response. Zhang *et al.*[38] have loaded various noble metal (Au, Pt, Pt/Au) catalysts on Fe_2O_3 powders using lysine as a linker. Because, lysine also acts as a capping agent to stabilize small Au or Pt particles, a high degree of noble metal dispersion could be also achieved. In the present study, the Pt catalyst was loaded during the solvothermal reaction of the solution containing lysine. Thus, the dual roles of lysine as a linker and a capping agent will be advantageous in the uniform and convenient loading of noble metal catalyst on the surface of sensing materials.

Li-ion battery

The cycling performance of solvothermally synthesized, hollow Fe_2O_3 spheres between the voltage range of 0.01–3.0 (V *vs.* Li/Li^+) at a current density of 100 mA g^{-1} is shown in Fig. 7. The high initial discharge capacity of 2165 mA h g^{-1} far exceeded the theoretical capacity of Fe_2O_3 (1038 mA h g^{-1}),[39] as has been widely reported for transition metal oxides.[39–42] This excessive capacity is ascribed to the electrolyte reduction at low voltage to form a solid electrolyte interphase and interfacial lithium

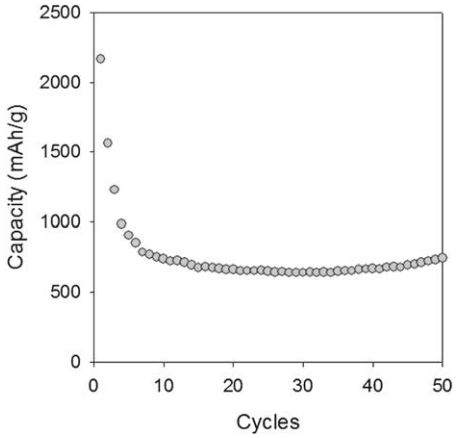

Fig. 7 The cycling performance of the electrode using Fe_2O_3 hollow spheres heat-treated at 450 °C for 2 h between the voltage range of 0.01 and 3.0 (V *vs.* Li/Li^+) at a current density of 100 mA g^{-1}.

storage.[43,44] However, the discharge/charge capacity becomes quite stable after the first 10 cycles at a specific discharge capacity of 650 mA h g^{-1} with a coulombic efficiency of around 98%. Even after 50 cycles, a specific discharge capacity of 648 mA h g^{-1} was delivered, which indicates the good stability of the hollow Fe_2O_3 spheres electrode. The much higher stabilized capacity (650 mA h g^{-1}) compared to the theoretical capacity of graphite (372 mA h g^{-1}) presents these Fe_2O_3 hollow spheres as a promising anode candidate for lithium ions batteries.

In general, to achieve high performance in Li-ion battery, the electrode materials should have high surface area, short distance for Li^+ ion transport, and freedom for volume change.[45] The high capacity and good cycle stability in our case were attributed to the novel hollow sphere structure. Fig. 4c and d clearly shows the large space between the inner spheres and the outer shells, which can facilitate the electrolyte penetration and increase the interfacial area between the electrode and electrolyte. Furthermore, the hollow spheres can expand or shrink freely to accommodate the volume changes during the lithium intercalation and deintercalation process, resulting in reduced structural damage.

The Fe_2O_3 hollow sphere electrode presented here showed better electrochemical stability than a Fe_2O_3 nanotube electrode which retains 514 mA h g^{-1} after 100 cycles at 100 mA g^{-1}.[31] Furthermore, it exhibited better performance than the 414 mA h g^{-1} after 60 cycles reported for Fe_2O_3 spheres with solid inner structures (current density: 100 mA g^{-1}).[39] And it possessed similar performance to the Fe_2O_3 nanoflakes reported by Reddy *et al.* (current density: 65 mA g^{-1}).[46] Considering the facile solvothermal synthesis, these Fe_2O_3 hollow spheres are a promising anode candidate in Li-ion battery applications.

Conclusions

Well-defined Fe_3O_4 hollow spheres were prepared by amino acid-mediated solvothermal reaction, and were successfully converted into nearly monodisperse Fe_2O_3 hollow spheres with the nanoscale thickness (20–30 nm) of shells by heat treatment at 500 °C for 2 h. Both hollow spheres contained a small sphere within the large shell. In the as-prepared Fe_3O_4 hollow spheres, a significant amount of nitrogen was detected not only in the small sphere within the large shell but also in the space between the small sphere and the large shell. In contrast, the nitrogen content was negligible in the heat-treated Fe_2O_3 hollow spheres. The connection between the inner sphere and the outer shell was observed in the cross-sectional image of the Fe_3O_4 hollow spheres prepared by focused ion beam treatment. The Fe_3O_4 hollow spheres were formed by lysine-mediated, solvothermal self-assembly reaction. The heat-treated Fe_2O_3 hollow spheres showed enhanced C_2H_5OH sensing characteristics in comparison to the counterparts such as Fe_2O_3 spheres with solid inner structures and agglomerated nanoparticles, and exhibited a high and promising Li-intercalation behaviour. These enhancements were attributed to the effective diffusion of analyte gas or Li-ion onto the entire materials *via* the nanoscale shells.

Acknowledgements

This work was supported by the Korea Science and Engineering Foundation (KOSEF) National Research Laboratory (NRL) program grant funded by the Korean government (MEST) (No.R0A-2008-000-20032-0).

References

1 P. Tartaj, T. González-Carreño and C. J. Serna, *Adv. Mater.*, 2004, **16**, 529–533.
2 Z. Wu, K. Yu, S. Zhang and Y. Xie, *J. Phys. Chem. C*, 2008, **112**, 11307–11313.
3 J. Liu, F. Liu, K. Gao, J. Wu and D. Xue, *J. Mater. Chem.*, 2009, **19**, 6073–6084.
4 Y. Piao, J. Kim, H. B. Na, D. Kim, J. S. Baek, M. K. Ko, J. H. Lee, M. Shokouhimehr and T. H. Hyeon, *Nat. Mater.*, 2008, **7**, 242–247.
5 S.-L. Chou, J.-Z. Wang, D. Wexler, K. Konstatinov, C. Zhong, H.-K. Liu and S.-X. Dou, *J. Mater. Chem.*, 2010, **20**, 2092–2098.
6 W. S. Choi, Y. Koo, Z. Zhongbin, Y. Li and D.-Y. Kim, *Adv. Funct. Mater.*, 2007, **17**, 1743–1749.
7 J.-H. Lee, *Sens. Actuators, B*, 2009, **140**, 319–336.
8 F. Gyger, M. Hüber, C. Feldmann, N. Barsan and U. Weimar, *Chem. Mater.*, 2010, **22**, 4821–4827.
9 S. Han, B. Jang, T. Kim, S. M. Oh and T. Hyeon, *Adv. Funct. Mater.*, 2005, **15**, 1845–1850.
10 F. Caruso, M. Spasova, A. Susha, M. Giersig and R. A. Caruso, *Chem. Mater.*, 2001, **13**, 109–116.
11 S.-J. Ding, C.-L. Zhang, M. Yang, X.-Z. Qu, Y.-F. Lu and Z.-Z. Yang, *Polymer*, 2006, **47**, 8360–8366.
12 H. Shiho and N. Kawahashi, *J. Colloid Interface Sci.*, 2000, **226**, 91–97.
13 M. Ohinishi, Y. Kozuka, Q.-L. Ye, H. Yoshikawa, K. Awaga, R. Matsuno, M. Kobayashi, A. Takahara, T. Yokoyama, S. Bandow and S. Iijima, *J. Mater. Chem.*, 2006, **16**, 3215–3220.
14 M.-M. Titirici, M. Antonietti and A. Thomas, *Chem. Mater.*, 2006, **18**, 3808–3812.
15 X. Chen, Z. Zhang, X. Li and C. Shi, *Chem. Phys. Lett.*, 2006, **422**, 294–298.
16 B. Mao, Z. Kang, E. Wang, C. Tian, Z. Zhang, C. Wang, Y. Song and M. J. Li, *J. Solid State Chem.*, 2007, **180**, 489–496.
17 S.-W. Cao and Y.-J. Zhu, *Acta Mater.*, 2009, **57**, 2154–2165.
18 J. H. Bang and K. S. Suslick, *J. Am. Chem. Soc.*, 2007, **129**, 2242–2243.
19 D. Du and M. Cao, *J. Phys. Chem. C*, 2008, **112**, 10754–10758.
20 W. Cheng, K. Tang, Y. Qi, J. Sheng and Z. Liu, *J. Mater. Chem.*, 2010, **20**, 1799–1805.
21 T. Yamashita and P. Hayes, *Appl. Surf. Sci.*, 2008, **254**, 2441–2449.
22 C. S. Love, A. R. Hirst, V. Chechik, D. K. Smith, I. Ashworth and C. Brennan, *Langmuir*, 2004, **20**, 6580.
23 A. R. Hirst and D. K. Smith, *Org. Biomol. Chem.*, 2004, **2**, 2965–2971.
24 O. Durupthy, J. Bill and F. Aldinger, *Cryst. Growth Des.*, 2008, **12**, 2696–2704.

25 J. Bandara, K. Tennakone and J. Kiwi, *Langmuir*, 2001, **17**, 3964–3969.
26 J. Zhu, O. K. Tan, Y. C. Lee, T. S. Zhang, B. Y. Tay and J. Ma, *Nanotechnology*, 2006, **17**, 5960–5969.
27 G. Cao, *Nanostructures and Nanomaterials*, Imperial College Press, London, 2004.
28 C. J. Martinez, B. Hockey, C. B. Montgomery and S. Semancik, *Langmuir*, 2005, **21**, 7937–7944.
29 H.-R. Kim, K.-I. Choi, J.-H. Lee and S. A. Akbar, *Sens. Actuators, B*, 2009, **136**, 138–143.
30 N. Yamazoe, G. Sakai and K. Shimanoe, *Catal. Surv. Asia*, 2003, **7**, 63–75.
31 J. Chen, L. Xu, W. Li and X. Gou, *Adv. Mater.*, 2005, **17**, 582–586.
32 X. Gou, G. Wang, X. Kong, D. Wexler, J. Horvat, J. Yang and J. Park, *Chem.–Eur. J.*, 2008, **14**, 5996–6002.
33 K.-I. Choi, H.-R. Kim and J.-H. Lee, *Sens. Actuators, B*, 2009, **138**, 497–503.
34 I.-D. Kim, A. Rothschild, T. Hyodo and H. L. Tuller, *Nano Lett.*, 2006, **6**, 193–198.
35 Q. Zhao, Y. Gao, X. Bai, C. Wu and Y. Xie, *Eur. J. Inorg. Chem.*, 2008, 1643–1648.
36 H.-R. Kim, K.-I. Choi, K.-M. Kim, I.-D. Kim, G. Cao and J.-H. Lee, *Chem. Commun.*, 2010, **46**, 5061–5063.
37 M. D'Arienzo, L. Armelao, A. Cacciamani, C. M. Mari, S. Polizzi, R. Ruffo, R. Scotti, A. Testino, L. Wahba and F. Morazzoni, *Chem. Mater.*, 2010, **22**, 4083–4089.
38 J. Zhang, X. Liu, X. Gou, S. Wu and S. Wang, *Chem.–Eur. J.*, 2010, **16**, 8108–8116.
39 X.-L. Wu, Y.-G. Guo, L.-J. Wan and C.-W. Hu, *J. Phys. Chem. C*, 2008, **112**, 16824–16829.
40 H. Morimoto, S.-I. Togishima and Y. Iizhuka, *J. Power Sources*, 2005, **146**, 315–318.
41 B. T. Hang, T. Doi, S. Okada and J.-I. Yamaki, *J. Power Sources*, 2007, **174**, 493–500.
42 S. Liu, L. Zhang, J. Zhou, J. Xiang, J. Sun and J. Guan, *Chem. Mater.*, 2008, **20**, 3623–3628.
43 P. Balaya, H. Li, L. Kienle and J. Maier, *Adv. Funct. Mater.*, 2003, **13**, 621–625.
44 J. Maier, *Nat. Mater.*, 2005, **4**, 805–815.
45 Y. Wang and G. Cao, *Adv. Mater.*, 2008, **20**, 2251–2269.
46 M. V. Reddy, Y. Yu, C.-H. Sow, X. Shen, C. T. Lim, G. V. S. Rao and B. V. R. Chowdari, *Adv. Mater.*, 2007, **17**, 2792–2799.